

# First-principles Calculation of the Electronic Structure and Optical Properties of ZnO Co-doped with Nb and Ta

Jinpeng WANG<sup>2</sup>, Tao SHEN<sup>1,2\*</sup>, Hongchen LIU<sup>3</sup>

<sup>1</sup> Key Laboratory of Engineering Dielectrics and Its Application, Ministry of Education, Harbin University of Science and Technology, Harbin, 150080, China

<sup>2</sup> College of Science, Harbin University of Science and Technology, Harbin, 150080, China

<sup>3</sup> School of Electrical Engineering and Automation, Harbin Institute of Technology, Harbin, 150001, China

crossref <http://dx.doi.org/10.5755/j01.ms.25.3.19956>

Received 16 January 2018; accepted 09 April 2018

First-principle calculations have been performed to investigate the electronic structure and optical properties of ZnO co-doped with Nb and Ta. The three doping structures are set to:  $Zn_{0.9375}Nb_{0.0625}O$ ,  $Zn_{0.9375}Ta_{0.0625}O$  and  $Zn_{0.875}Nb_{0.0625}Ta_{0.0625}O$ . The experiments show that co-doping with Nb and Ta narrows the band gap. And it causes the Fermi level to shift upwards and enter the conduction band, while enhancing the conductivity of the doped system. In addition, it has been determined that the dielectric imaginary part of the dopant system is larger than that of the pure ZnO in the low energy region. The absorption side of the dopant system, on the other hand, exhibits a redshift. Furthermore, the transmittance of the ultraviolet region is significantly increased, and the function loss spectrum appears to redshift. This will provide a good theoretical basis for the study and the applications of photoelectric materials co-doped with Nb and Ta.

**Keywords:** ZnO co-doped with Nb and Ta, first-principles calculation, electronic structure, optical properties.

## 1. INTRODUCTION

In recent years, ZnO has attracted the attention of researchers, becoming another research hotspot, due to its superior properties as a short wavelength semiconductor material. ZnO, a direct bandgap semiconductor material of II–VI, has an energy gap width of 3.37 eV at room temperature and an exciton binding energy of up to 60 meV [1, 2]. In addition to its stable chemical properties and excellent photoelectric properties [3], ZnO also exhibits a direct band gap, large exciton binding energy, and controllable defects energy level; as a result, ZnO-based semiconductors are recognized as a very promising photonic material in the ultraviolet (UV) and visible regions [4, 5]. Because of these superior properties, ZnO has a number of applications in various fields, including transparent conductor films, solar cells, varistors, gas sensors, photo- and electro-luminescent devices, piezoelectric devices, photoconductors, thermoelectric devices, scintillation and UV sensors [6–12].

Currently, studies have focused on aspects of ZnO's applications as thin film coatings on photovoltaic devices. Studies have been performed to modify the optical properties of ZnO by doping different kinds of elements, at different proportions. For example, it has been demonstrated by Khan et al. that the optical absorption spectra for Zr-doped ZnO nanoparticles lies within the visible region [13]. Likewise, another study [14] has determined that the electronic structure and ferromagnetic stability of Cu-doped ZnO have changed significantly after doping. Furthermore, other studies have found that replacing the Zn atom with Ag or Eu in the ZnO unit cell

allows for the tuning of its luminescence [15–17]. In addition, the metal element co-doped ZnO will have a significant impact on the nature of the change. Al–Na co-doped ZnO can improve dopant solubility, tailor the band structure of the matrix, and influence the formation of defects due to the charge compensations [18]. On the other hand, Al–Ga co-doped ZnO has shown better durability against humidity, when compared to Al-doped ZnO [19], while Ni and Li co-doped ZnO has shown a significantly enhanced ferromagnetism [20]. Therefore, due to the significant effects of doping on ZnO, the doping process of ZnO with various types of elements has been of major interest to researchers, both in the theoretical and experimental fields. This will, subsequently, allow for a more comprehensive understanding of the different changes in electronic structure and optical properties following the doping process of ZnO.

As VB family elements, V, Nb and Ta exhibit the most stable oxidation state,  $X + 5$  ( $X = V, Nb$  or  $Ta$ ), in natural environments. Thus, as multi-electron donors, V, Nb, and Ta are capable of improving the electrical conductivity of ZnO-based semiconductors, thereby altering their structure and optical properties. According to previous studies [21–27], good electrical conductivity and high levels of absorption in the visible light range have been observed in both V- and Nb-doped ZnO. Despite the extensive number of studies performed on ZnO-based semiconductors, researches on Nb- and Ta-doped ZnO are still very limited. Therefore, due to the nature of Nb and Ta, the fact that the electronic structure and the optical properties of ZnO are altered after being doped by the two elements, should not be neglected. The following study will, therefore, explore this change.

In this study, ZnO represents the matrix, while Nb and Ta are selected as the doping atoms. The first-principles

\* Corresponding author. Tel.: +86-0451-86390727;  
E-mail address: [taoshenchina@163.com](mailto:taoshenchina@163.com) (T. Shen)

ultrasoft pseudopotential is, then, applied to compare the changes in the band structure and optical properties of the crystals before and after Nb- and Ta-doping of ZnO. Analysis of the intrinsic causes of this study is then performed, while the results obtained from the analysis can provide a theoretical reference for subsequent researches that are to be performed on ZnO.

## 2. MODEL AND COMPUTATIONAL METHODS

Density function theory (DFT) calculation was performed within the generalized gradient approximation (GGA), with the correction of Perdew-Burke-Ernzerhof (PBE) to account for the exchange-correction potential as employed in the software of Cambridge Sequential Total Energy Package (CASTEP) Code of Materials Studio, and used the method of plane-wave pseudopotentials [28, 29]. In addition, the Materials Visualizer was employed to build the ZnO model.

The ideal structure of ZnO exhibits a hexagonal wurtzite crystal structure with the corresponding space group symmetry of P63mc, with the primitive cell parameters listed as follows:  $a = b = 0.3249$  nm,  $c = 0.5204$  nm,  $\alpha = \beta = 90^\circ$ , and  $\gamma = 120^\circ$  [30]. Based on the primitive cell, a  $2 \times 2 \times 2$  ZnO supercell was constructed as the model of the ZnO. Fig. 1 a and b shows a Nb-doped ZnO (ZnO:Al), which corresponds to  $\text{Zn}_{0.9375}\text{Nb}_{0.0625}\text{O}$ , with one Nb atom substituting one of the Zn atoms. Figure 1(c), on the other hand, shows a Ta-doped ZnO (ZnO:Ta) which corresponds to  $\text{Zn}_{0.9375}\text{Nb}_{0.0625}\text{O}$ , where one Nb atom substitutes one Zn atom. Likewise, Fig. 1 d represents the model of ZnO co-doped with Nb and Ta (ZnO:Nb-Ta) which corresponds to  $\text{Zn}_{0.875}\text{Nb}_{0.0625}\text{Ta}_{0.0625}\text{O}$ , in which one Nb atom substitutes one Zn atom, and one Ta atom substitutes another one of the Zn atoms.

In addition, ultrasoft pseudopotentials are used to replace the nuclei. The electronic valance configurations for each of the atomic species were denoted as: Zn-3d104s2, O-2s22p4, Nb-4d45s1, and Ta-5d36s2. After

performing a careful convergence test and contrast, the cutoff energy of the plane wave was assumed as 460 eV. Brillouin zone wavevector  $k$  points were then performed over a  $4 \times 4 \times 2$  grid size which was generated automatically by the Monkhorst-Pack method [31]. Furthermore, during the optimization process, a total energy convergence of  $0.5 \times 10^{-6}$  eV/atom, Hellmann-Feynman ionic force of 0.001 eV/nm, maximum stress of 0.02 Pa, and maximum displacement of  $0.5 \times 10^{-5}$  nm have been applied. Additionally, the scissors operation has been carried out in the optical absorption of ZnO in order to obtain the exact values of the optical absorption spectra within low energy ranges.

## 3. RESULTS AND DISCUSSION

### 3.1. Results of optimized structure

In order to determine the feasibility of the experimental data, we optimized the equilibrium structure using experimental methods and related parameters which were mentioned in Model and computational methods. Table 1 shows the experimental and calculated lattice constants, and the volume  $V$  of ZnO. Additionally, the lattice parameters of optimized ZnO doped systems have also been compared with ZnO lattice parameters in several papers which used the same experimental principle. Exp.a, Exp.b, Exp.c, respectively, is the data in different references. Cal.d is the lattice parameter before optimization, and Cal.e is lattice parameter obtained after calculation and optimization. The lattice constant which we calculated  $a$  and  $c$ , and the volume  $V$  of pure ZnO, and Nb-, Ta-, and ZnO co-doped with Nb and Ta, are shown in Table 2. As shown in Table 1, the parametric values, after optimization, of  $a$  and  $c$  were calculated as 3.272 and 5.261 respectively, which are in good agreement with the experimental values [2, 30, 32, 33]. Meanwhile, it can be perceived that the lattice constants of doped ZnO increased gradually, as shown in Table 2.

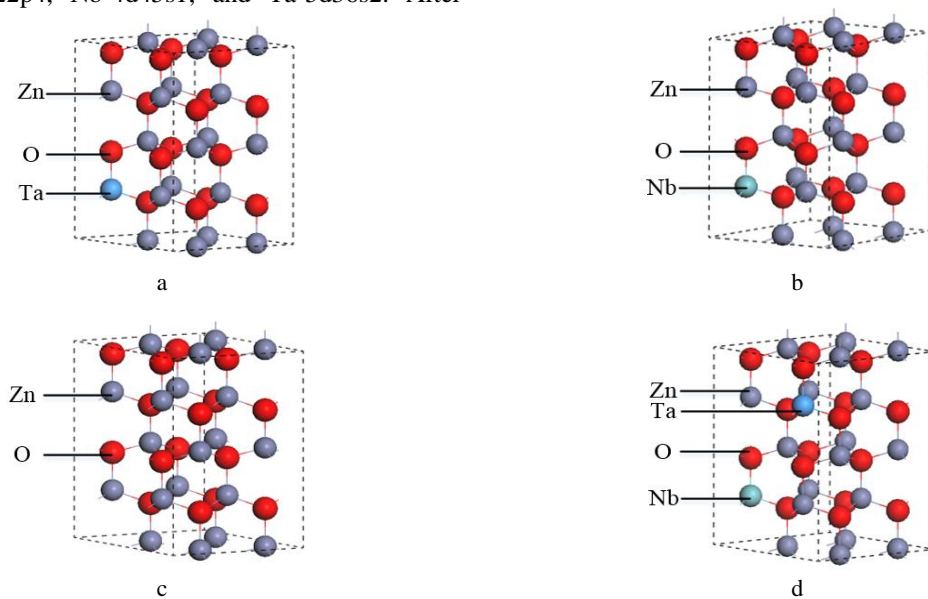


**Fig. 1.** Schematic of the structures of ZnO ( $2 \times 2 \times 2$ ) supercells: a – ZnO; b –  $\text{Zn}_{0.9375}\text{Nb}_{0.0625}\text{O}$ ; c –  $\text{Zn}_{0.9375}\text{Ta}_{0.0625}\text{O}$ ; d –  $\text{Zn}_{0.875}\text{Nb}_{0.0625}\text{Ta}_{0.0625}\text{O}$

**Table 1.** Experimental and calculated lattice constants, ( $a = b, c$ ), and volume  $V$  of ZnO

	$a, \text{nm}$	$c, \text{nm}$	$V, \text{nm}^3$	$c/a$
Exp.a [2]	0.3283	0.5311	$49.573 \times 10^{-3}$	1.618
Exp.b [32]	0.3247	0.5203	$47.506 \times 10^{-3}$	1.602
Exp.c [33]	0.3278	0.5295	$49.274 \times 10^{-3}$	1.615
Cal.d [30]	0.3249	0.5204	$47.574 \times 10^{-3}$	1.602
Cal. e (Present Study)	0.3272	0.5261	$48.778 \times 10^{-3}$	1.608

**Table 2.** Lattice constants  $a$  and  $c$  and volume  $V$  of pure ZnO, Nb-, Ta-, ZnO co-doped with Nb and Ta

	$a, \text{nm}$	$c, \text{nm}$	$V, \text{nm}^3$	$c/a$
Pure ZnO	3.272	5.261	$48.778 \times 10^{-3}$	1.608
Zn <sub>0.9375</sub> Nb <sub>0.0625</sub> O	3.379	5.492	$54.305 \times 10^{-3}$	1.625
Zn <sub>0.9375</sub> Ta <sub>0.0625</sub> O	3.381	5.571	$55.151 \times 10^{-3}$	1.648
Zn <sub>0.875</sub> Nb <sub>0.0625</sub> Ta <sub>0.0625</sub> O	3.458	5.779	$59.846 \times 10^{-3}$	1.671

According to the results, the Nb-doped ZnO and Ta-doped ZnO show the least lattice distortion and doping feasibility. On the contrary, ZnO co-doped with Nb and Ta exhibits serious lattice distortion and unacceptable mismatch with + 0.0186 nm and + 0.0518 nm for  $a$  and  $c$  respectively; these discrepancies may be attributed to the large ionic radius of Nb<sup>5+</sup> and Ta<sup>5+</sup>. Even so, it was determined that the changes of ZnO co-doped with Nb and Ta observed in the values of  $a$  and  $c$  are still in an allowable range. Thus, we can clearly observe that the Nb-doped ZnO, Ta-doped ZnO, and ZnO co-doped with Nb and Ta exhibit feasibility. The results obtained are, therefore, consistent with literature on Nb-doped ZnO, as reported by Shaw et al. [34], and on Ta-doped ZnO, as reported by Wu et al. [35].

### 3.2. Band structure

The band structures of pure ZnO and ZnO doped systems are shown in Fig. 2. Because the nature of the

material is mainly determined by the change in the vicinity of the Fermi level, caused by the doping of ZnO, the Fermi level at zero energy, and at  $-8$  to  $8$  eV of the band structure are shown in Fig. 2. Fig. 2 a shows the band structure of pure ZnO. As observed, the ZnO-semiconductor exhibits a direct band gap due to its valence band at the top and bottom of the conduction bands, which are located at point G in Fig. 2 a. Additionally, the band gap width is determined as 0.804 eV. The result obtained is in close agreement with those calculated by Si X et al. [36] at 0.731 eV. However, this is still far from the band gap with a value of 3.37 eV, for pure ZnO, and this difference can be attributed to the generally low phenomenon in the calculation of band gaps present in DFT. For pure ZnOs, the energy of Zn 3d is overestimated, which leads to its enhanced interaction with O 2p, and as a result, the band gap's bandwidth becomes larger, hence the lowering of the band gap. Despite the underestimation of the band-gap, the optical spectrum is predicted well by the DFT calculation [37]. A common way of fixing the underestimated band gap is to apply a rigid energy shift to the computed Kohn-Sham spectra, which is called a scissor operation.

It can be seen from Fig. 2 that the maximum values of the valence band and the minimum values of the conduction band in the three cases of the ZnO doping still remain at point G. This means that the doped ZnO still belongs to the category of direct band gap oxides. Moreover, it has also been determined that Nb-doped ZnO, Ta-doped ZnO, and ZnO co-doped with Nb and Ta band gaps are narrow, and the degree of narrowing of the co-doped conditions is the greatest at 0.664 eV, 0.671 eV and 0.614 eV respectively. Thus, the conductivity of ZnO, after doping, was enhanced. In addition, we can also determine that the conduction and valence bands of the doped systems move downwards, correspondingly.

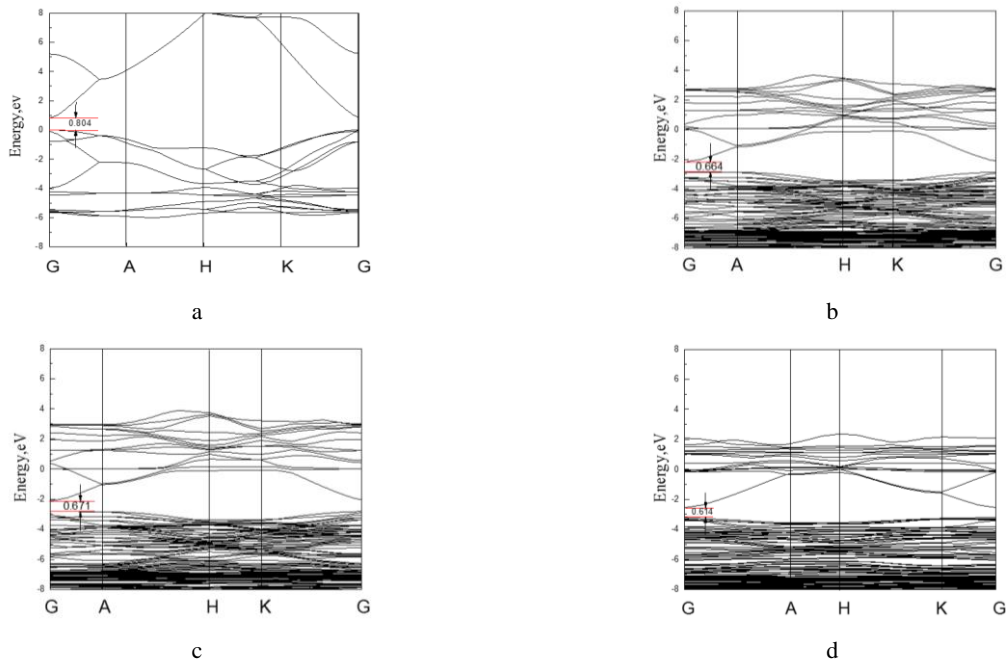


**Fig. 2.** Band structures of pure ZnO and ZnO doped systems: a – ZnO; b – Nb-ZnO; c – Ta-ZnO; d – (Nb, Ta)-ZnO

### 3.3. Density of states

Fig. 3 shows the total density of states (TDOS) and partial density of states (PDOS) of the pure ZnO and ZnO doping systems. As observed in Fig. 2 a, the valence band of pure ZnO can be divided into three parts. Within the range of  $-4.41$  to  $0$  eV, it is mainly composed of O 2p and small amounts of Zn 3d states. On the other hand, valence bands within the range of  $-6.63$  to  $4.41$  eV are mainly composed of Zn 3d and partial O 2p states. Lastly, an isolated band in the range of  $-18.3$  to  $16.5$  eV at the valence band is formed with O 2s state. The composition of conduction bands, on the other hand, is consistent with the total density of ZnO in that they are mainly formed by the Zn 4s and the O 2p states.

The TDOS and PDOS of the ZnO doping systems are shown in Fig. 3 b–d). As observed, the Fermi level is shifted upwards, and into the conduction band after doping, as the doping of Nb and Ta elements leads to an increase in conductive carriers. This also leads to enhanced conductivity of the systems after doping, especially after co-doping. In Fig. 3 b, we can see that there exists an impurity level near the Fermi level, after doping Nb, which is caused by the Nb 4d state, and as a result, causes the conduction band width to become smaller. In addition, there are two isolated bands in the range of  $-58.0$  to  $-56.7$  eV and  $-34.3$  to  $-32.6$  eV at the valence band, which is formed by the Nb 5s and 4p states. Nonetheless, these are far from the Fermi level, and, therefore, the impact is small and does not require significant consideration.

As shown in Fig. 3 c, the effects on the Fermi level is attributed to the Ta 5d state after doping, and is mainly composed of the Ta 5d and the partial O 2p states at the valence band between  $-1.32$  and  $3.76$  eV. Since the 4s

electrons of Zn and 5d electrons of Ta are decreasing and increasing, respectively, the contribution of Zn in the conduction band is gradually weakened.

Fig. 3 d shows the TDOS and PDOS of ZnO co-doped with Nb and Ta. After co-doping, the s orbital electron density of Nb and Ta has very little influence on the valence and conduction bands of the ZnO crystal, and only functions at a deeper level ( $< -30$  eV). The maximum effect on the bottom of the conduction band and the top of the valence band are still attributed to the Nb 4d and Ta 5d states.

According to the analyses made above, in ZnO co-doped with Nb and Ta, the interactions between the impurity atoms will narrow down the forbidden band width, while shifting the Fermi level upwards. At the same time, the quantum state close to the bottom of the conduction band has been occupied by electrons, whereby the degeneration of carriers takes place to form degenerate semiconductors. This, therefore, obtains n-type semiconductors which exhibit better electrical properties.

### 3.4. Optical properties

#### 3.4.1. Dielectric function

The dielectric function can reflect the information between the energy band structure and the optical spectrum of the solid, and can characterize the physical properties of the material. The macroscopic optical response function is usually described by the complex permittivity  $\varepsilon(\omega)$  of light, where  $\varepsilon(\omega) = \varepsilon_1(\omega) + i\varepsilon_2(\omega)$ . Where,  $\omega$  denotes the frequency, and  $\varepsilon_1(\omega)$  and  $\varepsilon_2(\omega)$  represent the real and imaginary parts of the dielectric function, respectively.

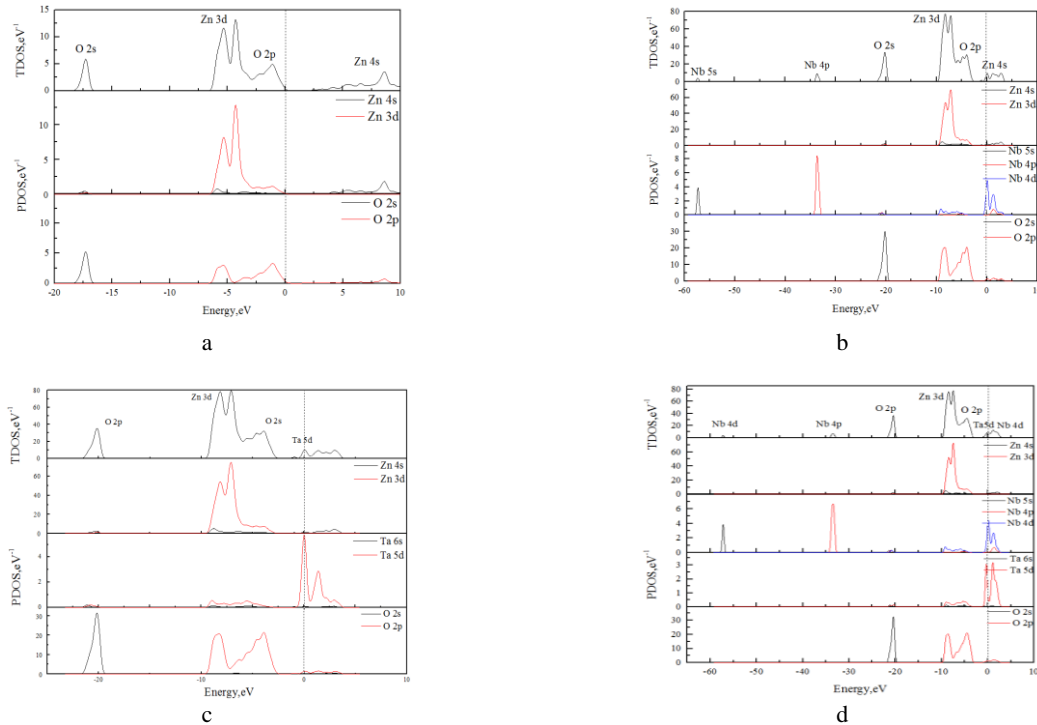


**Fig. 3.** TDOS and PDOS of pure ZnO and ZnO doping systems, where the Fermi level is set to 0: a – ZnO, b – Nb-ZnO; c – Ta-ZnO; d – (Nb, Ta)-ZnO

According to the definition of Kramers-Kronig dispersion relation and direct transition probability, we can deduce the real part  $\varepsilon_1$  and the imaginary part  $\varepsilon_2$  of the crystal dielectric function. The results are as follows:

$$\varepsilon_1(\omega) = 1 + c_2 \sum_{c,v} \int_{BZ} d^3k \frac{2}{2\pi} \frac{|e \cdot M_{cv}(k)|^2}{[E_c(k) - E_v(k)]}; \quad (1)$$

$$\times \frac{\hbar^3}{[E_c(k) - E_v(k)]^2 - \hbar^2 \omega^2}$$

$$\varepsilon_2(\omega) = \frac{4\pi^2}{m^2 \omega^2} \sum_{c,v} \int_{BZ} d^2k \frac{2}{2\pi} |e \cdot M_{cv}(k)|^2 \times \delta[E_c(k) - E_v(k) - \hbar\omega] \quad (2)$$

In the equation,  $\hbar = h/2\pi$ ,  $m$ ,  $e$ , and  $\omega$  represent the free electron mass, free electron charge, and incident photon frequency, respectively. And where,  $c$ ,  $v$ ,  $BZ$ ,  $k$ , and  $|e \cdot M_{cv}(k)|^2$  denote the conduction band, valence band, first Brillouin zone, reciprocal lattice vector, and the momentum transition matrix element, respectively, while  $E_c(k)$  represents the conduction band on the intrinsic level, and  $E_v(k)$  is the valence band on the intrinsic level.

Since the imaginary part  $\varepsilon_2$  of the crystal dielectric function describes the energy required for the transition of the electron from the valence band to the conduction band, we only analyze the imaginary part of the dielectric function. Fig. 4 shows the pure ZnO and the doped ZnO dielectric functions of the imaginary part. As shown in Fig. 4, when compared to pure ZnO, the imaginary part of the dielectric function becomes smooth after doping the impurity atoms. There is only one larger dielectric peak, between 2.68 and 2.85 eV. This corresponds to the direct transitions between O 2p, Nb 4d, and Ta 5d states in the state density map. A rise in the dielectric peaks are observed in all Nb-doped ZnO, Ta-doped ZnO, and ZnO co-doped with Nb and Ta systems.

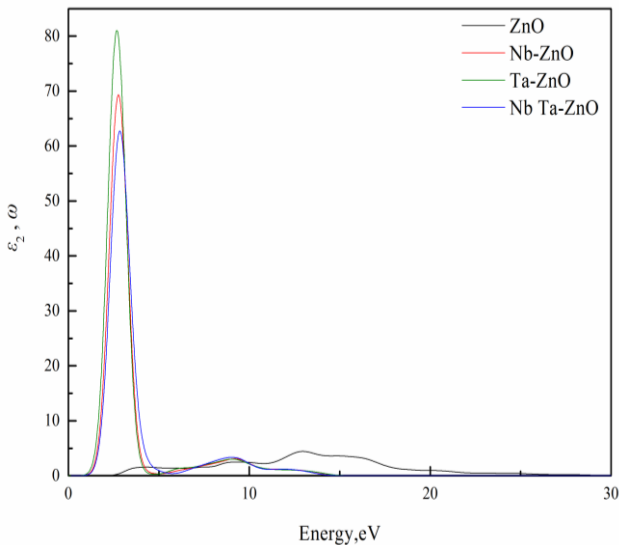


**Fig. 4.** Intrinsic ZnO and the doping ZnO dielectric function of the imaginary part  $\varepsilon_2$

In Nb and Ta co-doped ZnO, the dielectric peak moves slightly towards the high energy direction. This is due to the fact that the Fermi level enters the conduction band after the impurity is doped on the ZnO, therefore, the conduction band is filled with electrons at the Fermi level. This results in the transition of the electronic valence band to the Fermi level and above, hence increasing the required energy. Furthermore, in the case of ZnO co-doped with Nb and Ta, the interaction between the Nb atom and the Ta atom causes the energy required for the electron transition to be less than the energy required for a single doping, hence the lower value of the peak of co-doping relative to that of the single doping peak, with a range between 2.68 and 2.85 eV.

### 3.4.2. Absorption

The absorption spectrum can reflect the absorption versus wavelength loops of the doped ZnO to different wavelengths of light [38, 39]. The absorption coefficient can be directly derived from  $\varepsilon_1(\omega)$  and  $\varepsilon_2(\omega)$ . The form of expression [40] is as follows:

$$I(\omega) = \sqrt{2}\omega \left[ \sqrt{\varepsilon_1^2(\omega) - \varepsilon_2^2(\omega)} - \varepsilon_1(\omega) \right]^{1/2} \quad (3)$$

The absorption coefficient of pure ZnO and doped ZnO is shown in Fig.5. There are three distinct absorption peaks in pure ZnO, located at 10.07 eV, 16.87 eV, and 20.69 eV. After the incorporation of impurities, the absorption peak decreases, especially in Nb and Ta co-doped ZnO. The absorption peak is mainly derived from the transition of the valence band to the electron band in the excited state, while the weakening of the absorption peak indicates that the reduction of the transition process is due to the incorporation of Nb and Ta impurity atoms. In addition, since the new impurity band is introduced after doping, a new absorption peak appears in the low energy region. Moreover, it is clearly perceived that the absorption side exhibits a redshift phenomenon as the doping of Nb and Ta atoms leads to a reduction in the forbidden band width.

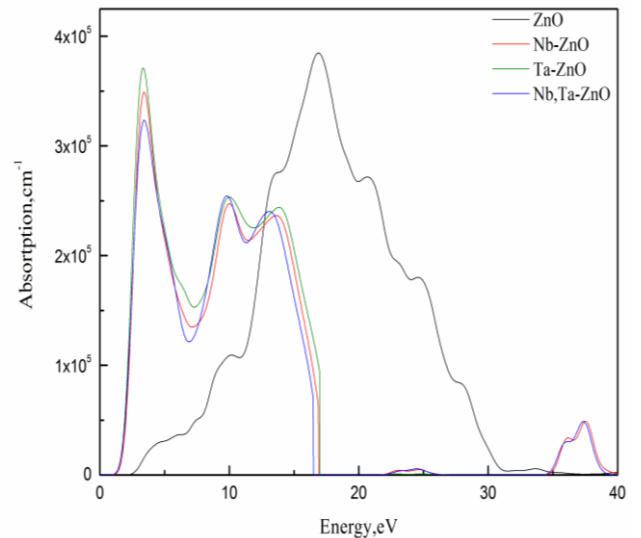


**Fig. 5.** The absorption coefficients of pure ZnO and doped ZnO

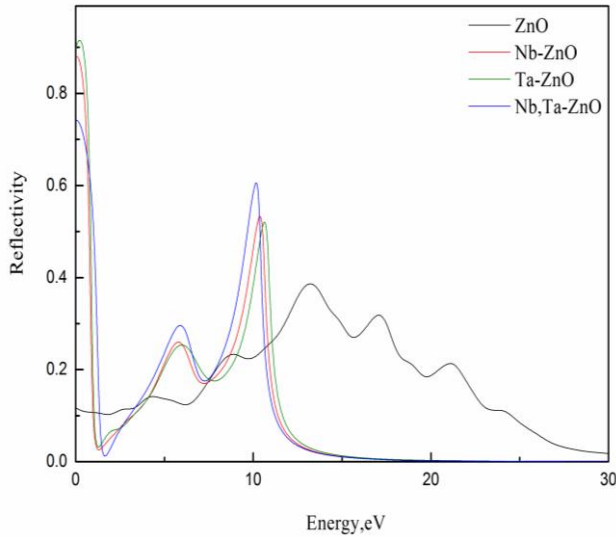


**Fig. 6.** The reflectivity of pure ZnO and doped ZnO

This is mainly due to the energy structures of Nb and Ta elements, which significantly improves the absorption property of ZnO after doping.

### 3.1.3. Reflectivity

The change in reflectivity is observed before and after ZnO doping, as shown in Fig. 6. The main peak of the reflection of pure ZnO is located close to a value of 13.24 eV. After doping, the main peak moves towards the low energy region. Nb and Ta co-doped ZnO has the largest variation in this case. Although the trend is decreasing in the high energy region, the reflectivity of the high energy region after doping of Nb and Ta is lower than that of pure ZnO. And the doped ZnO decreased its absorption and reflectivity in the 20–30 eV high-energy region. This implies that the transmittance of the ultraviolet region in the 20–30 eV high-energy region after doping of Nb and Ta elements is significantly increased, especially when Nb and Ta is co-doped with ZnO. In addition, Nb and Ta co-doped ZnO systems has the lowest reflectivity in the visible range. However, the reflectivity of ZnO-doped systems in the low-energy UV region increases again to the highest level.

### 3.1.4. Loss function

The energy loss spectrum is a physical quantity that describes the loss of energy of electrons through uniform dielectrics. The loss function  $L(\omega)$ , is described in terms of  $\varepsilon_1(\omega)$  and  $\varepsilon_2(\omega)$  as:

$$L(\omega) = \varepsilon_2(\omega) \left[ \varepsilon_1^2(\omega) + \varepsilon_2^2(\omega) \right]. \quad (4)$$

As shown in Fig. 7, the energy-loss peak of pure ZnO is close to a value of 14.35 eV. In this case of doping, the energy loss peak appears redshift, where the energy-loss peak of Nb and Ta co-doped ZnO has the largest redshift. It is clearly seen that two energy loss peaks are present after doping; this corresponds to the two sharp descending segments of the reflection spectrum in Fig. 6.

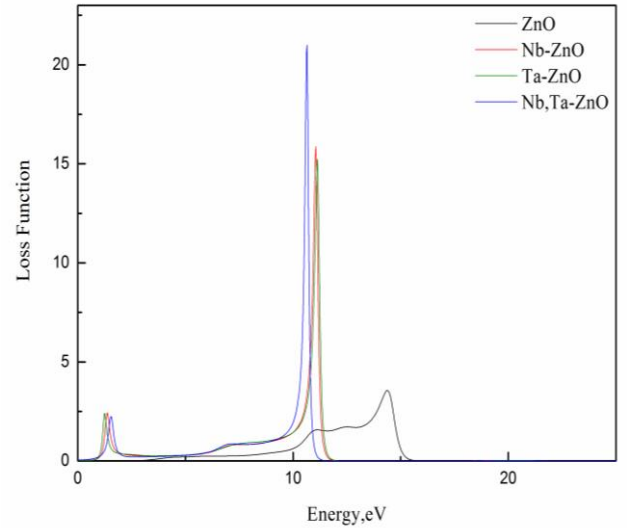


**Fig. 7.** The loss function of pure ZnO and doped ZnO

## 4. CONCLUSIONS

The electronic structure and optical properties of ZnO co-doped with Nb and Ta have been investigated using the first-principles ultrasoft pseudopotential within GGA. A summary of our results are as follows:

1. In this study, the direct band gap of the ZnO was determined as 0.804 eV. After doping, the forbidden band width becomes smaller, and the co-doped band gap is the smallest.
2. After doping, impurity atoms provide free carriers near the Fermi level, while the Fermi level shifts upwards into the conduction band. This significantly improves the conductivity of the dopant system.
3. In terms of optical properties, the dielectric imaginary part of the dopant system is larger than the pure ZnO in the low energy region.
4. The absorption side of the dopant system exhibits a redshift phenomenon. Meanwhile, the doping system still has different degrees of absorption when the energy is higher than 34.69 eV.
5. After doping of Nb and Ta elements, the transmittance of the ultraviolet region is significantly increased in the 20–30 eV high-energy region, especially when Nb and Ta is co-doped with ZnO. Nb and Ta co-doped ZnO systems has the lowest reflectivity in the visible range. And the reflectivity of ZnO-doped systems in the low-energy UV region increases again to the highest level.
6. The function loss spectrum appears redshift and the energy-loss peak of Nb and Ta co-doped ZnO has the largest redshift.

## Acknowledgments

This work was supported by the National Natural Science Foundation of China [grant number 51677044] and the Outstanding Youth Innovation Foundation of Harbin [grant number 2017RAYXJ022].

## REFERENCES

1. **Li, Y., Zhao, X., Fan, W.** Structural, Electronic, and Optical Properties of Ag-Doped ZnO Nanowires: First Principles Study *Journal of Physical Chemistry C* 115 (9) 2011: pp. 3552–3557.  
<https://doi.org/10.1021/jp1098816>
2. **Li, L., Wang, W., Liu, H., Liu, X., Song, Q., Ren, S.** First Principles Calculations of Electronic Band Structure and Optical Properties of Cr-Doped ZnO *The Journal of Physical Chemistry C* 113 (19) 2009: pp. 8460–8464.  
<https://doi.org/10.1021/jp811507r>
3. **Zhou, Z., Komori, T., Ayukawa, T., Yukawa, H., Morinaga, M., Koizumi, A., Takeda, Y.** Li- and Er-codoped ZnO with Enhanced 1.54  $\mu\text{m}$  Photoemission *Applied Physics Letters* 87 (9) 2005: pp. 091109.  
<https://doi.org/10.1063/1.2035867>
4. **Reynolds, D.C., Look, D.C., Jogai, B., Collins, T.C.** Polariton and Free-exciton-like Photoluminescence in ZnO *Applied Physics Letters* 79 (2; 43) 2001: pp. 3794.  
<https://doi.org/10.1063/1.1412435>
5. **Gopal, P., Spaldin, N.A.** Magnetic Interactions in Transition-metal-doped ZnO: An Ab Initio Study *Physical Review B* 74 (9) 2006: pp. 094418.  
<https://doi.org/10.1103/PhysRevB.74.094418>
6. **Erhart, P., Albe, K.** First-principles Study of Migration Mechanisms and Diffusion of Oxygen in Zinc Oxide *Physical Review B* 73 (11) 2006: pp. 115207.  
<https://doi.org/10.1103/PhysRevB.73.115207>
7. **Chuang, C.-H.-M., Brown, P.-R., Bulović, V., Bawendi, M.-G.** Improved Performance and Stability in Quantum dot Solar Cells through Band Alignment Engineering *Nature Materials* 13 (8) 2014: pp. 796–801.  
<https://doi.org/10.1038/nmat3984>
8. **Iwata, K., Tampo, H., Yamada, A., Fons, P., Matsubara, K., Sakurai, K., Ishizuka, S., Niki, S.** Growth of ZnO and Device Applications *Applied Surface Science* 244 (1) 2005: pp. 504–510.  
<https://doi.org/10.1016/j.apsusc.2004.10.109>
9. **Esro, M., Vourlias, G., Somerton, C., Milne, W.I., Adamopoulos, G.** High-mobility ZnO Thin Film Transistors Based on Solution-processed Hafnium Oxide Gate Dielectrics *Advanced Functional Materials* 25 (1) 2015: pp. 134–141.  
<https://doi.org/10.1002/adfm.201402684>
10. **Amrani, A.El., Hijazi, F., Lucas, B., Boucle, J., Aldissi, M.** Electronic Transport and Optical Properties of Thin Oxide Films *Thin Solid Films* 518 (16) 2010: pp. 4582–4585.  
<https://doi.org/10.1016/j.tsf.2009.12.036>
11. **Rackauskas, S., Klimova, O., Jiang, H., Nikitenko, A., Chernenko, K.A., Shandakov, S.D., Kauppinen, E.I., Tolochko, O.V., Nasibulin, A.G.** A Novel Method for Continuous Synthesis of ZnO Tetrapods *The Journal of Physical Chemistry C* 119 (28) 2015: pp. 16366–16373.  
<https://doi.org/10.1021/acs.jpcc.5b03702>
12. **Rackauskas, S., Mustonen, K., Järvinen, T., Mattila, M., Klimova, O., Jiang, H., Tolochko, O., Lipsanen, H., Kauppinen, E.I., Nasibulin, A.G.** Synthesis of ZnO Tetrapods for Flexible and Transparent UV Sensors *Nanotechnology* 23 (9) 2012: pp. 095502.  
<https://doi.org/10.1088/0957-4484/23/9/095502>
13. **Khan, I., Khan, S., Nongjai, R., Ahmed, H., Khan, W.** Structural and Optical Properties of Gel-combustion Synthesized Zr Doped ZnO Nanoparticles *Optical Materials* 35 (6) 2013: pp. 1189–1193.  
<https://doi.org/10.1016/j.optmat.2013.01.019>
14. **Huang, L.M., Rosa, A.L., Ahuja, R.** Ferromagnetism in Cu-doped ZnO from First-principles Theory *Physical Review B* 74 (7) 2006: pp. 075206.  
<https://doi.org/10.1103/PhysRevB.74.075206>
15. **Duan, L., Lin, B., Zhang, W., Zhong, S., Fu, Z.** Enhancement of Ultraviolet Emissions from ZnO Films by Ag Doping *Applied Physics Letters* 88 (23) 2006: pp. 232110.  
<https://doi.org/10.1063/1.2211053>
16. **Wang, X.B., Song, C., Geng, K.W., Zeng, F., Pan, F.** Luminescence and Raman Scattering Properties of Ag-Doped ZnO Films *Journal of Physics D: Applied Physics* 39 (23) 2006: pp. 4992.  
<https://doi.org/10.1088/0022-3727/39/23/014>
17. **Pan, H., Yi, J.B., Shen, L., Wu, R.Q., Yang, J.H., Lin, J.Y., Feng, Y.P., Ding, J., van, L.H., Yin, J.H.** Room-Temperature Ferromagnetism in Carbon-doped ZnO *Physical Review Letters* 99 (12) 2007: pp. 127201.  
<https://doi.org/10.1103/PhysRevLett.99.127201>
18. **Wang, T., Liu, Y., Fang, Q., Wu, M., Sun, X., Lu, F.** Low Temperature Synthesis Wide Optical Band Gap Al and (Al, Na) Co-doped ZnO Thin Films *Applied Surface Science* 257 (6) 2011: pp. 2341–2345.  
<https://doi.org/10.1016/j.apsusc.2010.09.100>
19. **Lee, W., Shin, S., Jung, D.R., Kim, J., Nahm, C., Moon, T., Park, B.** Investigation of Electronic and Optical Properties in Al–Ga Codoped ZnO Thin Films *Current Applied Physics* 12 (3) 2012: pp. 628–631.  
<https://doi.org/10.1016/j.cap.2011.09.008>
20. **Pei, G., Xia, C., Wu, B., Wang, T., Zhang, L., Dong, Y., Xu, J.** Studies of Magnetic Interactions in Ni-doped ZnO from First-principles Calculations *Computational Materials Science* 43 (3) 2008: pp. 489–494.  
<https://doi.org/10.1016/j.commatsci.2007.12.012>
21. **Liu, S.H., Huang, J.C.A., Lin, C.R., Qi, X.** Electrical Transport and ac Conductivity Properties of Hydrogenated Annealing V-doped ZnO *Journal of Applied Physics* 105 (7) 2009: pp. 07C502.  
<https://doi.org/10.1063/1.3055274>
22. **Shao, J.Z., Dong, W.W., Li, D., Tao, R.H., Deng, Z.H., Wang, T., Meng, G., Zhou, S., Fang, X.D.** Metal-semiconductor Transition in Nb-doped ZnO Thin Films Prepared by Pulsed Laser Deposition *Thin Solid Films* 518 (18) 2010: pp. 5288–5291.  
<https://doi.org/10.1016/j.tsf.2010.04.068>
23. **Lin, J.M., Zhang, Y.Z., Ye, Z.Z., Gu, X.Q., Pan, X.H., Yang, Y.F., Lu, J.G., He, H.P., Zhao, B.H.** Nb-doped ZnO Transparent Conducting Films Fabricated by Pulsed Laser Deposition *Applied Surface Science* 255 (13) 2009: pp. 6460–6463.  
<https://doi.org/10.1016/j.apsusc.2009.01.002>
24. **Gokulakrishnan, V., Parthiban, S., Jeganathan, K., Ramamurthi, K.** Structural, Optical, and Electrical Properties of Nb-Doped ZnO Thin Films Prepared by Spray Pyrolysis Method *Journal of Electronic Materials* 40 (12) 2011: pp. 2382.  
<https://doi.org/10.1007/s11664-011-1755-1>
25. **Xu, J.W., Wang, H., Jiang, M.H., Liu, X.Y.** Properties of Nb-doped ZnO Transparent Conductive Thin Films Deposited by Rf Magnetron Sputtering Using a High Quality Ceramic Target *Bulletin of Materials Science* 33 (2) 2010: pp. 119–122.

- <https://doi.org/10.1007/s12034-010-0016-x>
26. **Wang, L., Meng, L., Teixeira, V., Song, S., Xu, Z., Xu, X.** Structure and Optical Properties of ZnO: V Thin Films with Different Doping Concentrations *Thin Solid Films* 517 (13) 2009: pp. 3721–3725.  
<https://doi.org/10.1016/j.tsf.2008.12.043>
  27. **Krithiga, R., Chandrasekaran, G.** Synthesis, Structural and Optical Properties of Vanadium Doped Zinc Oxide Nanograins *Journal of Crystal Growth* 311 (21) 2009: pp. 4610–4614.  
<https://doi.org/10.1016/j.jcrysgro.2009.08.033>
  28. **Perdew, J.P., Chevary, J.A., Vosko, S.H., Jackson, K.A., Pederson, M.R., Singh, D.J., Fiolhais, C.** Atoms, Molecules, Solids, and Surfaces: Applications of the Generalized Gradient Approximation for Exchange and Correlation *Physical Review B* 46 (11) 1992: pp. 6671.  
<https://doi.org/10.1103/PhysRevB.46.6671>
  29. **Segall, M.-D., Lindan, P.-J., Probert, M.-A., Pickard, C.-J., Hasnip, P.-J., Clark, S.-J., Payne, M.-C.** First-principles Simulation: Ideas, Illustrations and the CASTEP Code *Journal of Physics: Condensed Matter* 14 (11) 2002: pp. 2717.  
<https://doi.org/10.1088/0953-8984/14/11/301>
  30. **Abbassi, A., El Amrani, A., Ez-Zahraouy, H., Benyoussef, A., El Amraoui, Y.** First-principles Study on the Electronic and Optical Properties of Si and Al Co-doped Zinc Oxide for Solar Cell Devices *Applied Physics A* 122 (6) 2016: pp. 584.  
<https://doi.org/10.1007/s00339-016-0111-y>
  31. **Monkhorst, H.J., Pack, J.D.** Special Points for Brillouin-Zone Integrations *Physical Review B* 13 (12) 1976: pp. 5188.  
<https://doi.org/10.1103/physrevb.13.5188>
  32. **Mahmood, A., Tezcan, F., Kardaş, G., Karadağ, F.** Effect of Sr Doping on the Electronic Band Structure and Optical Properties of ZnO: A First Principle Calculation *Journal of Applied Physics* 122 (11) 2017: pp. 113102.  
<https://doi.org/10.1063/1.5002075>
  33. **Li, Y., Zhao, X., Fan, W.** Structural, Electronic, and Optical Properties of Ag-doped ZnO Nanowires: First Principles Study *The Journal of Physical Chemistry C* 115 (9) 2011: pp. 3552–3557.  
<https://doi.org/10.1021/jp1098816>
  34. **Shaw, A., Wrench, J.S., Jin, J.D., Whittles, T.J., Mitrovic, I.Z., Raja, M., Dhanak, V.R., Chalker, P.R., Hall, S.** Atomic Layer Deposition of Nb-doped ZnO for Thin Film Transistors *Applied Physics Letters* 109 (22) 2016: pp. 222103.  
<https://doi.org/10.1063/1.4968194>
  35. **Wu, Y., Li, C., Li, M., Li, H., Xu, S., Wu, X., Yang, B.** Microstructural and Optical Properties of Ta-doped ZnO Films Prepared by Radio Frequency Magnetron Sputtering *Ceramics International* 42 (9) 2016: pp. 10847–10853.  
<https://doi.org/10.1016/j.ceramint.2016.03.214>
  36. **Si, X., Liu, Y., Wu, X., Lei, W., Xu, J., Du, W., Zhou, T., Lin, J.** The Interaction between Oxygen Vacancies and Doping Atoms in ZnO *Materials & Design* 87 2015: pp. 969–973.  
<https://doi.org/10.1016/j.matdes.2015.08.027>
  37. **Bechstedt, F., Tenelsen, K., Adolph, B., Del Sole, R.** Compensation of Dynamical Quasiparticle and Vertex Corrections in Optical Spectra *Physical Review Letters* 78 (8) 1997: pp. 1528.  
<https://doi.org/10.1103/PhysRevLett.78.1528>
  38. **Si, X., Liu, Y., Wu, X., Lei, W., Lin, J., Gao, T., Zheng, L.** Al–Mg Co-doping Effect on Optical and Magnetic Properties of ZnO Nanopowders *Physics Letters A* 379 (22–23) 2015: pp. 1445–1448.  
<https://doi.org/10.1016/j.physleta.2015.03.025>
  39. **Lu, X., Liu, Y., Si, X., Shen, Y., Yu, W., Wang, W., Luo, X., Zhou, T.** Temperature-Dependence on the Structural, Optical, And Magnetic Properties of Al-Doped ZnO Nanoparticles *Optical Materials* 62 2016: pp. 335–340.  
<https://doi.org/10.1016/j.optmat.2016.09.037>
  40. **Jin, Z., Qiao, L., Guo, C., He, Z., Liu, L., Rong, M.** First-principle Study of Electrical and Optical Properties of (Al, Sn) Co-doped ZnO *Optik-International Journal for Light and Electron Optics* 127 (4) 2016: pp. 1988–1992.  
<https://doi.org/10.1016/j.ijleo.2015.10.224>